2023 IEEE/RSJ International Conference on Intelligent Robots and Systems (IROS)
October 1-5, 2023. Detroit, USA

The MyoPassivity Puzzle: How Does Muscle Fatigue Affect Energetic Behavior of the Human Upper-limb During Physical Interaction with Robots?

Suzanne Oliver, *Student Member, IEEE*, Peter Paik*, *Student Member, IEEE*,
Xingyuan Zhou*, *Student Member, IEEE*, S. Farokh Atashzar†, *Senior Member, IEEE*

2023 IEEE/RSJ International Conference on Intelligent Robots and Systems (IROS) | 978-1-6654-9190-7/23/$31.00 ©2023 IEEE | DOI: 10.1109/IROS55552.2023.10341902

***Abstract*— The human limb possesses a remarkable capacity to absorb energy during physical human-robot interaction (pHRI), which can be quantified as the biomechanical "Excess of Passivity" (EoP) using non-linear control theory. This biomechanical passivity index can be used to reduce conservatism and increase the transparency of pHRI stabilizers. Previous work on EoP has used system identification techniques to compute EoP offline. However, for use in real-time controllers, an instantaneous method for EoP estimation would be desired. This paper hypothesizes that muscle fatigue can potentially be a complicating factor which can cumulatively affect the ability of human biomechanics to absorb mechanical energy over time during physical interaction with robots. In this work, we focused on the energetic behavior of the human wrist during pHRI, and, for the first time, we investigated the effect of fatigue on EoP. The EoP for five participants was computed throughout one hundred-second trials of high-frequency wrist perturbations in four directions. Subjects maintained a stiff and consistent grip throughout each trial, causing an accumulation of fatigue in the forearm muscles. Muscle activity was recorded using an array of sixteen sEMG sensors. It was found that the EoP degraded (in a statistically significant manner) with increased muscle fatigue in all directions, even when the level of muscle co-contraction was controlled consistently through a visual myofeedback mechanism. 100% of the subjects exhibited this decline in energy absorption capacity in all directions studied. The median drop in EoP after one-hundred seconds of perturbation was 11% for trials in the abduction and adduction directions and 22% in the pronation and supination directions. These results indicate a need for more robust estimation methods or new modalities to account for muscle fatigue in the control architectures of physical human-robot interaction.**

I. Introduction

Human-centered robotics (HCR) is a rapidly growing field, with a wide range of applications, from HCR for manufacturing and maintenance to telerobotics for medicine [1]–[5]. More specifically, haptics-enabled HCR systems and physically collaborative and interactive robots open new doors for expanding the applications, improving the user experience, and enhancing the capabilities of HCR systems. For example, haptic feedback has been shown to boost the performance of surgical robots [6], [7], and physically assistive rehabilitation, telerehabilitation, and exoskeleton systems have shown great potential for post-stroke therapy [8], [9].

When designing HCR systems with a physical Human-Robot Interaction (pHRI) component, two major issues should be addressed. First, the system must guarantee the stability of the interaction between the human and the robot. Second, the quality of the energy exchange between the human and the robot (which corresponds with the fidelity of force rendering) should be maximized. These goals for a pHRI system have been shown to be in conflict, meaning that a system with perfect transparency would be at the edge of instability. Stability can further be challenged if the communication channel is part of the loop of interaction due to issues such as delay, jitter, and packet loss, which have been shown to inject non-passive energy into the system [10], [11]. Additionally, some applications (such as assistive exoskeletons) require high forces to enable motions and escalate the energy in task conduction, and thus non-passive energy injections into the systems [12]. These stability issues would render the system unsafe for physical interaction with humans, so pHRI controllers impose stability at the expense of transparency, performance and fidelity of interaction.

Due to this limitation, much work has been done to improve the transparency of pHRI systems while ensuring the stability criterion is still met. One widely used method is the Time Domain Passivity Approach (TDPA), which adaptively injects damping into the system only when it detects non-passive energy exchanges [13]. In recent years, several improvements have been proposed to reduce the conservatism of this approach further [14]–[18].

One important but often overlooked factor that affects such stabilizers is the ability of the human limb to absorb energy from the robotic system during pHRI. Incorporating this capacity for energy absorption into the controller increases the energy margin of the system. This reduces the need for damping, thus allowing for higher fidelity of the energy exchange between the human and the robot. We have previously shown that utilizing even a fixed, conservative lower bound for the energy absorption capacity significantly improves the performance and transparency of telerobotic systems [19]–[22].

In order to model the intrinsic absorption capacity of the

Suzanne Oliver is with the Department of Mechanical and Aerospace Engineering, New York University (NYU), New York, NY, 11201 USA. Xingyuan Zhou and Peter Paik are with the Department of Electrical and Computer Engineering, NYU. S. Farokh Atashzar is with the Department of Electrical and Computer Engineering, Mechanical and Aerospace Engineering, Biomedical Engineering, NYU. Atashzar is also with NYU WIRELESS Center and NYU CUSP. This material is based upon work supported in part by the National Science Foundation awards #2208189 and #2121391. The work is also supported in part by GAANN Grant Number P200A210062.

* Xingyuan Zhou and Peter Paik contributed equally to this work and share the second authorship.

†Corresponding author: Atashzar (f.atashzar@nyu.edu).

Authorized licensed use limited to: New York University. Downloaded on September 08,2024 at 15:00:10 UTC from IEEE Xplore. Restrictions apply.

limb, we have previously proposed the use of "Excess of Passivity" (EoP) from non-linear control theory. In prior works, the EoP was calculated using offline methods, which require system identification and convergence over time [19]–[22]. These offline methods utilize force and motion sensors to calculate the EoP. To compute the EoP in real-time during pHRI, we cannot rely on the sensor measurements, as the force input from the human for task conduction (and the resulting velocity profile of the task) will be superimposed with the reactive forces and velocities of the user's biomechanics, rendering the problem unsolvable. Additionally, for real-time implementation, an instantaneous estimate for the EoP is preferable to waiting for the convergence of a system identification process from the sensor measurements. Thus, to achieve a real-time approximation of energy absorption capacity during a pHRI task, we look to other modalities to estimate the EoP.

One candidate modality for EoP estimation is muscle activation, measured using surface electromyography (sEMG). As a user's muscle activity increases, so does the viscoelasticity of the limb, which increases the damping effect on the system and, thus, the EoP [20], [23]. This increased muscle activity is also reflected in the sEMG signal, so sEMG can be seen as a candidate for EoP prediction. However, other factors, such as muscle fatigue, may also impact the EoP, and a method for real-time EoP estimation should be able to account for these changes.

This work is the first attempt to analyze the effect of muscle fatigue on the energetic behavior of the upper limb. To evaluate this change during muscle fatigue, a robust experiment was performed in this paper on five subjects. Each subject wore sixteen sEMG sensors on their forearm while holding tightly onto a robot handle and maintaining consistent sEMG (i.e., co-contraction) levels, using real-time visual myofeedback. The robot perturbed the participants' wrists at high frequencies in four directions (abduction, adduction, pronation, and supination) for one hundred seconds. Due to the subjects' stiff grip on the robot, their forearm muscles were fatigued during the task. The EoP was calculated using the system identification method, as described in [19]–[22] and the change in EoP as the subjects' fatigue increased was analyzed. It was found that the accumulation of fatigue consistently degraded the EoP for all subjects and all directions, even when the muscle co-contraction was controlled consistently through the visual myofeedback mechanism. This degradation in the energetic capacity of human biomechanics in pHRI was especially pronounced during perturbations in the pronation and supination directions. These findings, supported by a comprehensive statistical analysis given in the Results section, are reported here for the first time and indicate the need for more robust measures or new modalities for real-time EoP estimation using muscle activity information from sEMG sensors.

The rest of this paper is organized as follows. In Section II, we explain the mathematical bases for the identification of the EoP, the experimental setup, and data analysis. In Section III, the results of the paper are provided, and relevant discussions on the observations made are presented. Concluding remarks are given under Section IV.

II. Methods

A. Biomechanical Excess of Passivity

The mechanical coupling between the human wrist and robot handle during upper-limb pHRI can be viewed as a compounded dynamic system, including the human biomechanics, which are capable of absorbing interactional energy. For this, the output strictly passive (OSP) condition is used to define the margin of energy absorption:

$$\int_0^t U(t)^T Y(t)dt + E(0) \geq \xi \int_0^t Y(t)^T Y(t)dt, \quad (1)$$

where $U(t)$ is the input vector and $Y(t)$ is the output vector of the system. In robotics, the $E(0)$ term is typically assumed to be zero. When the coefficient ξ is non-negative, the system is output strictly passive, and ξ represents the excess of passivity. Such a system is L2 stable with a finite L2 gain equal to $1/\xi$ [24]. This numerical quantity provides the energy absorption margin of the human wrist during pHRI in the context of this paper. When ξ is negative, the system is output non-passive, and the ξ represents the shortage of passivity.

Using the OSP condition and an admittance framework, the EoP of the wrist can be quantified in an offline procedure using system identification. In this procedure, a pre-designed perturbation torque $\tau(t)$ is applied to the wrist, while the resulting angular velocity $\omega(t)$ is measured in different directions (e.g., pronation, supination, abduction, and adduction). In this context, the EoP is calculated by:

$$\hat{\xi} = \frac{\int_{T_i}^{T_f} \tau(t)^T \omega(t)dt}{\int_{T_i}^{T_f} \omega(t)^T \omega(t)dt}, \quad (2)$$

where T_i is the starting time and T_f is the finishing time of the perturbation window. Access to $\hat{\xi}$ during human-robot interaction can be exploited in the design of stabilizers used in pHRI as an additional information piece regarding the "margin of passivity" or an "embedded biomechanical energy tank" in the closed-loop passivity condition. Thus $\hat{\xi}$ can be used in reducing the conservatism of pHRI and enhancing haptic communication. As mentioned before, access to this information in real time is not feasible through the measurement of velocity and force signals as those inputs are occupied by the "task under conduction", and any additional perturbation (even an impulse) can be destructive and result in task conduction deficits. So it is indeed imperative to find other new modalities that can be used to predict this energetic characteristic instantaneously. Considering the function of the human musculoskeletal system, sEMG can be seen as a candidate, but as said before, it can be degraded due to fatigue. In this paper, through a novel experimental evaluation, we investigate the effect of fatigue on the changes in EoP when sEMG is kept consistent.

Authorized licensed use limited to: New York University. Downloaded on September 08,2024 at 15:00:10 UTC from IEEE Xplore. Restrictions apply.

B. Experimental Setup

Five healthy subjects (three males and two females, mean age 26.6 ± 3.6 years) participated in this study. The study was approved by the Institutional Review Board of New York University. Each subject signed a written consent form prior to participating in the experiment and denied any history of musculoskeletal injury. Demographic information about the subjects is shown in Table 1.

TABLE I
DEMOGRAPHIC DATA

Subject	Height (m)	Weight (kg)	Age	Sex
1	1.70	59	25	F
2	1.72	58	33	F
3	1.76	60	26	M
4	1.77	64	25	M
3	1.62	58	24	M

The experiment was designed to investigate the effect of muscle fatigue on EoP while maintaining consistent levels of muscle activation. Fig. 1 shows the design of the experiment. A Quansar High Definition Haptic Device (Quansar, Markham ON, Canada) robot was used to perturb the subject's hand and compute their EoP. Each trial consisted of perturbations in one of four directions: abduction, adduction, pronation, or supination, and lasted one hundred seconds. The perturbation signal was a mixed-frequency sinusoidal wave, with frequencies ranging from one to five Hertz. The perturbations were centered at fifteen degrees from neutral and oscillated from zero to thirty degrees in the given direction.The maximum magnitude of applied torque was 0.5 Newton-meters. The order of directions was randomized for each participant. Between trials, subjects were instructed to rest for fifteen minutes to recover from the muscle fatigue experienced during the trial.

Additionally, an array of sixteen wireless Bipolar Delsys Trignosystem (Delsys, Natick, MA, USA) sEMG sensors were placed on the forearm muscles of the subject, recording with a sampling rate of 1778 Hertz. Before beginning the experiment, the Maximum Voluntary Contraction (MVC) of the participant was recorded for two of the sensors. This information was used for visual myofeedback during the task. Sensors 11 and 15 (placed on the Extensor Carpi Ulnaris and Extensor Digitorum muscles, respectively) were chosen for this feedback due to their sensitivity to muscle contraction. The participants were shown real-time visual feedback of their sEMG levels for these two sensors as a percent of their MVC during the trial and were instructed to maintain thirty percent of the MVC throughout the task.

The posture and grip of the subject were also controlled. Participants were instructed to stand with their upper arm against their torso and bend their elbows at a ninety-degree angle. The robot was placed on a height-adjustable table to ensure the correct posture was feasible for all subjects. The

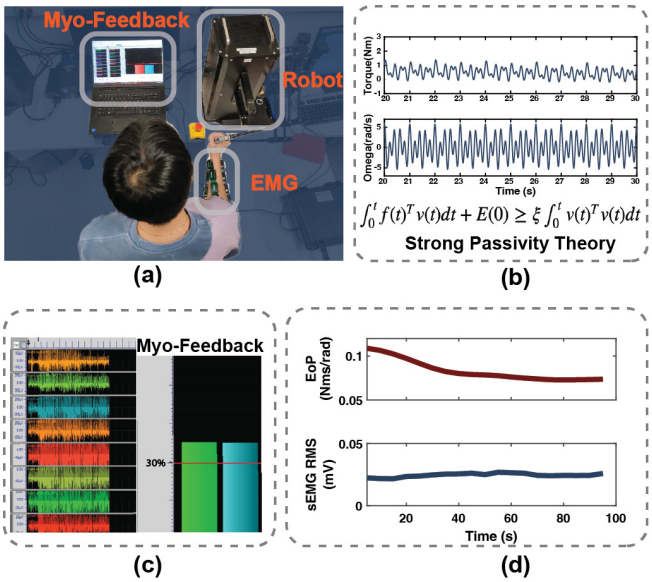

Fig. 1. (a) Experimental Setup, (b) Example of torque and angular velocity profiles, for use in EoP calculation, (c) Example of real-time visual myofeedback, and (d) Example of resulting EoP and sEMG RMS plots for Subject 2 in the pronation direction.

myofeedback was placed directly in front of the user to avoid twisting in the torso. Subjects were asked to grip the robot handle with their palm and all fingers in contact with the handle. During each trial, subjects were instructed to avoid voluntary motion, and the location of the handle was held constant. Fig. 2 shows the experimental setup.

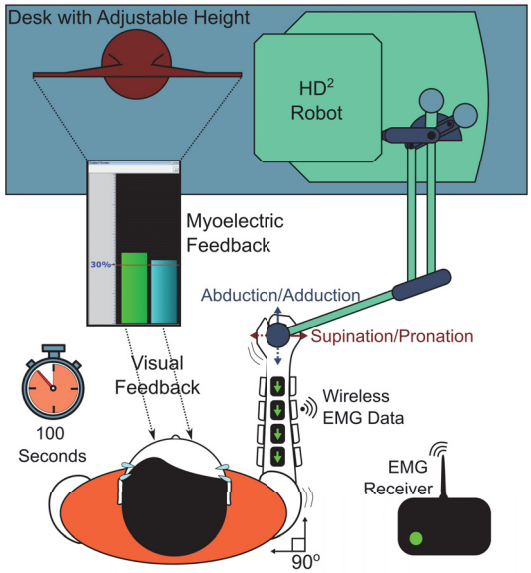

Fig. 2. Experimental setup showing the posture of the subject, high definition haptic robot, myofeedback bars, and Delsys wireless system and receiver.

C. Data Analysis

The data was processed in MATLAB. The sEMG data was first filtered using a 4th Order Butterworth bandpass

Authorized licensed use limited to: New York University. Downloaded on September 08,2024 at 15:00:10 UTC from IEEE Xplore. Restrictions apply.

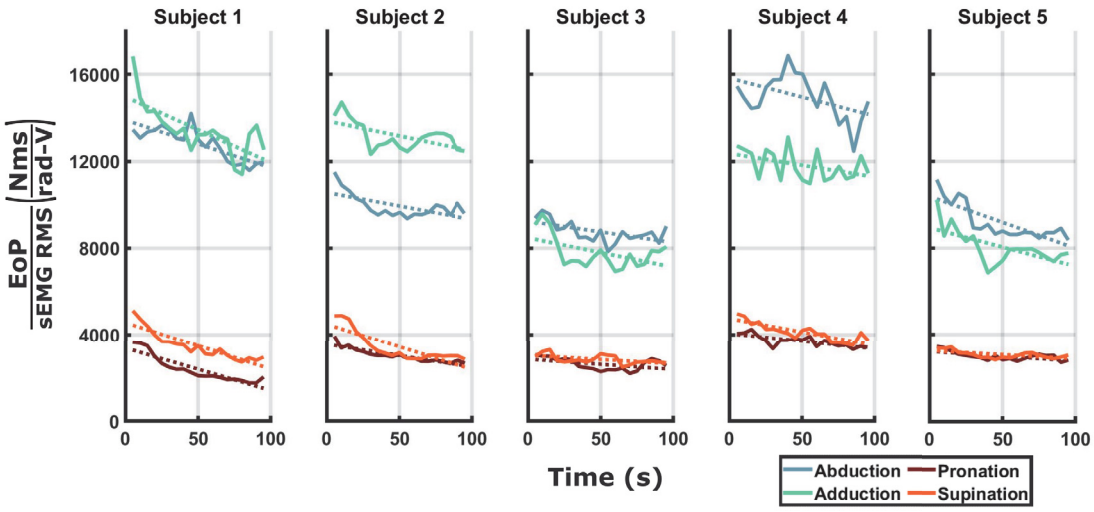

Fig. 3. The graphs represent $\frac{EoP}{sEMG\,RMS}$ trends over time for each subject and direction. The solid lines indicate the results at each time step and the corresponding dashed lines indicate the line of best fit in for each trial. The colors indicate the direction of perturbation.

filter between 20 and 100 Hertz. Additionally, line noise was filtered out with a 4th Order Butterworth bandstop filter between 58 and 62 Hertz. For each hundred-second trial, the first five seconds were disregarded due to an artifact in the EoP during rapid changes in direction.

The remaining data was segmented into five-second sections to analyze the changes over time. The Root-Mean-Square (RMS) of the sEMG data was calculated for each segment and each sEMG sensor. The RMS was computed using $\sqrt{\frac{1}{N}\sum_{i=1}^{N} X_i^2}$, where N is the number of points in the segment and X_i is the i^{th} point. This method was chosen to provide a metric of the signal magnitude of the sEMG, while reducing the sensitivity to noise by averaging over the segment. The mean of the RMS values over each sensor was taken for each segment to get a measure of the overall forearm muscle activity at each time step.

The EoP was calculated using the system identification approach based on the OSP formulation, as explained in Section II-A. The average over each five-second period was taken to monitor the changes over time. Since subjects could not perfectly control their muscle co-contraction using visual feedback, some variability around the targeted value of MVC percentage is expected even with the visual myofeedback provided during the task. To account for small fluctuations around the targeted co-contraction, the EoP was normalized at each time step with the corresponding sEMG RMS. This accounts for any fluctuations in muscle activity throughout the task. Secondly, in order to put the results of all subjects in a distribution and evaluate the changes, the $\frac{EoP}{sEMG\,RMS}$ values were normalized by the initial value for each subject-direction pair in order to track the changes over time and standardize across subjects.

Lastly, the distributions of $\frac{EoP}{sEMG\,RMS}$ values were compared after five seconds, thirty seconds, and one hundred seconds of perturbations to observe the effect of fatigue. Due to similarities in the values and the physical directionality, the abduction and adduction directions were paired for analysis, as were the pronation and supination directions. A Kolmogorov-Smirnov normality test was performed on the data, which rejected the null hypothesis (that the data is normally distributed) at a significance level of 0.05. As a result, the Wilcoxon signed-rank test was used to assess the significance of differences in the distributions at the time points, again with a significance level of 0.05.

III. Results

Fig. 3 shows the results of the $\frac{EoP}{sEMG\,RMS}$ trend over time for each subject. Each solid line represents a trial, and the corresponding dotted line shows the line of best fit of that trial. Notably, the slope of the line is negative for all subjects and in all directions. This result indicates that the $\frac{EoP}{sEMG\,RMS}$ value degrades as the muscles are fatigued and that this relationship exists for all four measured directions of perturbation.

It can also be seen that the values for abduction and adduction (A/A) are much larger than for pronation and supination (P/S) for all subjects, which is an interesting observation. Due to this disparity, the analysis of these pairs of perturbations was split for the remainder of this work.

The magnitude of the initial $\frac{EoP}{sEMG\,RMS}$ value depends on the biomechanics of the subject and the direction of perturbation. To more clearly visualize the trend over time, each $\frac{EoP}{sEMG\,RMS}$ value was normalized to the value at the first time segment for the given direction and subject. The results of this normalization are shown in Fig. 4 for A/A perturbations and Fig. 5 for P/S perturbations. The dashed lines indicate the trends for an individual subject and direction, while the solid line indicates the median value at each time point. The shaded region shows the area within one standard deviation of the median.

Both figures show a decrease in the median normalized $\frac{EoP}{sEMG\,RMS}$ over time. For the A/A case, the median normalized value after one hundred seconds of perturbations is

Authorized licensed use limited to: New York University. Downloaded on September 08,2024 at 15:00:10 UTC from IEEE Xplore. Restrictions apply.

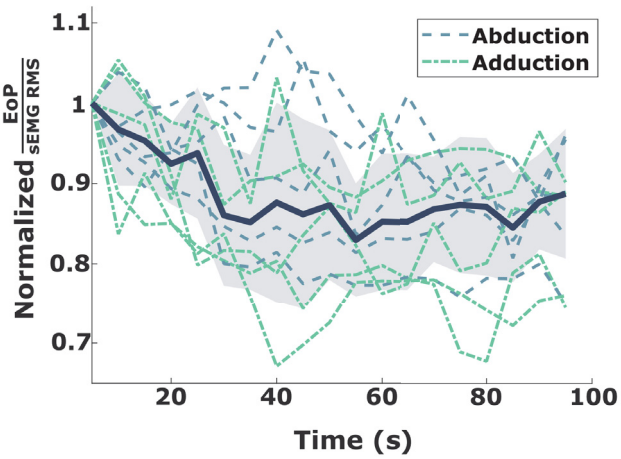

Fig. 4. Trend lines of normalized $\frac{EoP}{sEMG\,RMS}$ over time during perturbations in the abduction and adduction directions. The dashed lines indicate individual subject trends and the solid line is the median value at each time point. The shaded region indicates the standard deviation of the values, as a distance from the median.

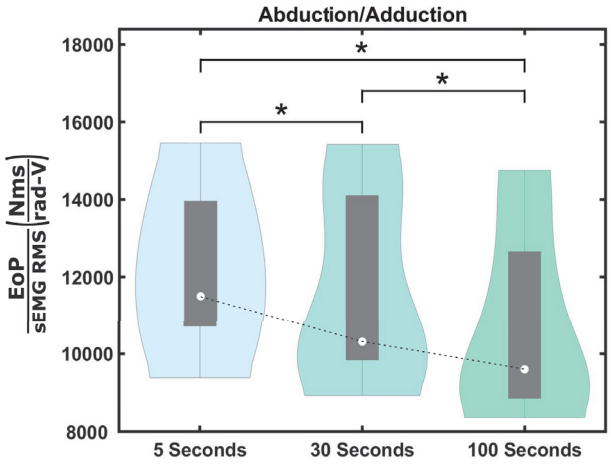

Fig. 6. Violin plots of $\frac{EoP}{sEMG\,RMS}$ distribution for perturbations in adduction and abduction directions after five seconds, thirty seconds and one-hundred seconds. The white circles indicate the median of each distribution and the dashed lines show the change in median value between distributions. Asterisks indicate a significant difference between the distributions for a 0.05 significance level.

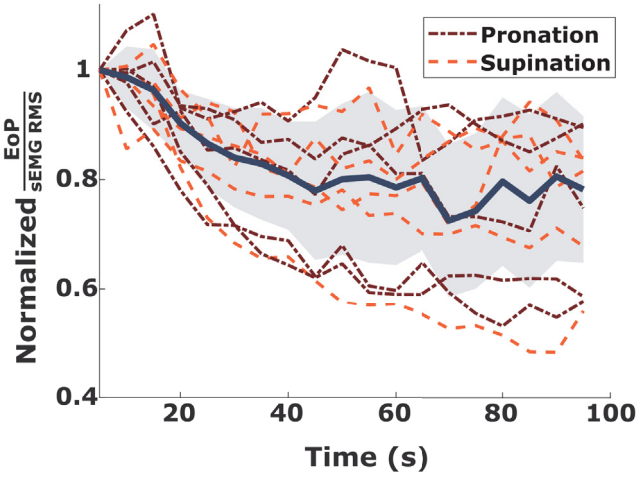

Fig. 5. Trend lines of normalized $\frac{EoP}{sEMG\,RMS}$ over time during perturbations in the pronation and supination directions. The dashed lines indicate individual subject trends and the solid line is the median value at each time point. The shaded area indicates the region plus or minus one standard deviation from the median.

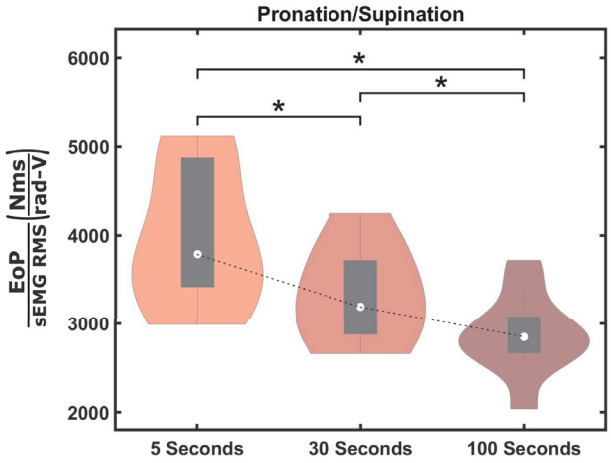

Fig. 7. Violin plots of $\frac{EoP}{sEMG\,RMS}$ distribution for perturbations in pronation and supination directions after five seconds, thirty seconds and one-hundred seconds. The white circles indicate the median of each distribution and the dashed lines show the change in median value between distributions. Asterisks indicate a significant difference between the distributions for a 0.05 significance level.

89% of the value after five seconds. The P/S case shows a larger drop, with a median of the normalized values at 78% of the five-second value after one hundred seconds. These results indicate an average decrease in energy absorption capacity of 11% for A/A and 22% for P/S. Interestingly, for both direction pairs, 100% of the participants conform to the median trend. In both plots, there is a steep decrease during the first thirty seconds of perturbation (with a median drop of 6% and 13% for A/A and P/S, respectively, after thirty seconds), then a less steep decline for the remainder of the time. The difference in the percentage drop between the P/S and A/A direction pairs may be due to the arm biomechanics, which are inherently less compliant in the A/A directions compared to the P/S directions.

Figs. 6 and 7 show the statistical analyses of the $\frac{EoP}{sEMG\,RMS}$ distributions, with Fig. 6 displaying the A/A directions and Fig. 7 showing the P/S directions. Both figures show violin plots of the $\frac{EoP}{sEMG\,RMS}$ values after five seconds, thirty seconds, and one-hundred seconds. As noted in the previous figures, the median values decrease as time elapses (and, therefore, as muscle fatigue increases). The differences are statistically significant between each distribution at the 0.05 significance level, per the Wilcoxon signed-rank test. This finding demonstrates, for the first time, that the energy absorption capability of the human upper-limb biomechanics, decoded using the passivity index (Excess of Passivity), degrades significantly as muscle fatigue accumulates. The

Authorized licensed use limited to: New York University. Downloaded on September 08,2024 at 15:00:10 UTC from IEEE Xplore. Restrictions apply.

observation holds even when accounting for fluctuations of muscle co-contractions around that targeted activation line. In other words, even when the subjects hold the muscle contraction around the same level of activation, the capacity of human biomechanics in the absorption of physical energy during pHRI would be reduced by fatigue accumulation. The results highlight the importance of detecting and tracking fatigue during pHRI and promote the design of new controllers that can track the effect of fatigue on the passivity of biomechanics when implementing the stability and safety of pHRI.

IV. Conclusion

In this study, the effect of muscle fatigue on the EoP of the human upper-limb was investigated for the first time. The goal of this work is to determine if fatigue degrades the inherent energy absorption capability of the limb. Incorporating EoP into a real-time controller could potentially reduce the conservatism necessary and allow for more transparent interactions during pHRI. However, in order to include EoP in real-time control, an instantaneous method of estimating it is required, which should be robust to muscle fatigue. In this work, we explore the effect of muscle fatigue on EoP normalized by the muscle activity recorded on an array of sixteen sEMG sensors.

Five healthy subjects participated in the experiment by completing four one-hundred-second trials of high-frequency wrist perturbations while fatiguing their forearm muscles by maintaining a stiff and consistent grip on the robot, measured via sEMG. It was found that the energy absorption capability of the limb declined for all perturbation directions in 100% of the subjects. Over a one-hundred-second period, the median decline was over 10% for perturbations in the A/A direction and over 20% for the P/S direction. Statistical analysis showed that the differences between the $\frac{EoP}{sEMG\,RMS}$ distributions at five seconds, thirty seconds, and one-hundred seconds were significantly different for both direction pairs. This result indicates that the sEMG RMS alone is not sufficient to predict the EoP of the limb when muscle fatigue can be a factor. More sophisticated metrics or other modalities for EoP estimation are called for to account for fatigue. Future work on this topic will include investigating the robustness of other modalities to fatigue and incorporating the findings of this study into a controller for pHRI .

References

[1] W. Baicun, X. Yuan, Y. Jianlin, Y. Xiaoying, and Z. Yuan, "Human-centered intelligent manufacturing: overview and perspectives," *Strategic Study of CAE*, vol. 22, no. 04, p. 139, 2020.

[2] V. Colla, R. Matino, A. J. Schröder, M. Schivalocchi, and L. Romaniello, "Human-centered robotic development in the steel shop: Improving health, safety and digital skills at the workplace," *Metals*, vol. 11, no. 4, p. 647, 2021.

[3] M. D. Parre and B. Sujatha, "Novel human-centered robotics: towards an automated process for neurorehabilitation," *Neurology research international*, vol. 2021, 2021.

[4] G. Niemeyer, C. Preusche, S. Stramigioli, and D. Lee, "Telerobotics," *Springer handbook of robotics*, pp. 1085–1108, 2016.

[5] W. Tian, M. Fan, C. Zeng, Y. Liu, D. He, and Q. Zhang, "Telerobotic spinal surgery based on 5g network: the first 12 cases," *Neurospine*, vol. 17, no. 1, p. 114, 2020.

[6] B. Weber and C. Eichberger, "The benefits of haptic feedback in telesurgery and other teleoperation systems: a meta-analysis," in *Universal Access in Human-Computer Interaction. Access to Learning, Health and Well-Being: 9th International Conference, UAHCI 2015, Held as Part of HCI International 2015, Los Angeles, CA, USA, August 2-7, 2015, Proceedings, Part III 9*, pp. 394–405, Springer, 2015.

[7] R. V. Patel, S. F. Atashzar, and M. Tavakoli, "Haptic feedback and force-based teleoperation in surgical robotics," *Proceedings of the IEEE*, vol. 110, no. 7, pp. 1012–1027, 2022.

[8] S. A. Ali, M. F. Miskon, A. Shukor, M. B. Bahar, and M. Q. Mohammed, "Review on application of haptic in robotic rehabilitation technology," *Int J Appl Eng Res*, vol. 12, no. 12, pp. 3203–3213, 2017.

[9] I. Bortone, D. Leonardis, N. Mastronicola, A. Crecchi, L. Bonfiglio, C. Procopio, M. Solazzi, and A. Frisoli, "Wearable haptics and immersive virtual reality rehabilitation training in children with neuromotor impairments," *IEEE Transactions on Neural Systems and Rehabilitation Engineering*, vol. 26, no. 7, pp. 1469–1478, 2018.

[10] K. Hashtrudi-Zaad and S. E. Salcudean, "Transparency in time-delayed systems and the effect of local force feedback for transparent teleoperation," *IEEE Transactions on Robotics and Automation*, vol. 18, no. 1, pp. 108–114, 2002.

[11] G. Niemeyer and J.-J. E. Slotine, "Telemanipulation with time delays," *The International Journal of Robotics Research*, vol. 23, no. 9, pp. 873–890, 2004.

[12] G. C. Thomas, J. M. Coholich, and L. Sentis, "Compliance shaping for control of strength amplification exoskeletons with elastic cuffs," in *2019 IEEE/ASME International Conference on Advanced Intelligent Mechatronics (AIM)*, pp. 1199–1206, IEEE, 2019.

[13] B. Hannaford and J.-H. Ryu, "Time-domain passivity control of haptic interfaces," *IEEE transactions on Robotics and Automation*, vol. 18, no. 1, pp. 1–10, 2002.

[14] J.-H. Ryu and C. Preusche, "Stable bilateral control of teleoperators under time-varying communication delay: Time domain passivity approach," in *Proceedings 2007 IEEE international conference on robotics and automation*, pp. 3508–3513, IEEE, 2007.

[15] H. Choi, R. Balachandran, and J.-H. Ryu, "Chattering-free time domain passivity approach," *IEEE Transactions on Haptics*, vol. 15, no. 3, pp. 572–581, 2022.

[16] M. Panzirsch, J.-H. Ryu, and M. Ferre, "Reducing the conservatism of the time domain passivity approach through consideration of energy reflection in delayed coupled network systems," *Mechatronics*, vol. 58, pp. 58–69, 2019.

[17] M. Panzirsch, H. Singh, and C. Ott, "The 6-dof implementation of the energy-reflection based time domain passivity approach with preservation of physical coupling behavior," *IEEE Robotics and Automation Letters*, vol. 5, no. 4, pp. 6756–6763, 2020.

[18] N. Feizi, R. V. Patel, M. R. Kermani, and S. F. Atashzar, "Adaptive wave reconstruction through regulated-bmflc for transparency-enhanced telerobotics over delayed networks," *IEEE Transactions on Robotics*, vol. 38, no. 5, pp. 2928–2942, 2022.

[19] S. F. Atashzar, M. Shahbazi, M. Tavakoli, and R. V. Patel, "A passivity-based approach for stable patient–robot interaction in haptics-enabled rehabilitation systems: modulated time-domain passivity control," *IEEE Transactions on Control Systems Technology*, vol. 25, no. 3, pp. 991–1006, 2016.

[20] S. F. Atashzar, M. Shahbazi, M. Tavakoli, and R. V. Patel, "A grasp-based passivity signature for haptics-enabled human-robot interaction: Application to design of a new safety mechanism for robotic rehabilitation," *The International Journal of Robotics Research*, vol. 36, no. 5-7, pp. 778–799, 2017.

[21] S. F. Atashzar, H.-Y. Huang, F. Del Duca, E. Burdet, and D. Farina, "Energetic passivity decoding of human hip joint for physical human-robot interaction," *IEEE Robotics and Automation Letters*, vol. 5, no. 4, pp. 5953–5960, 2020.

[22] P. Paik, S. Thudi, and S. F. Atashzar, "Power-based velocity-domain variable structure passivity signature control for physical human-(tele) robot interaction," *IEEE Transactions on Robotics*, 2022.

[23] P. H. McCrea, J. J. Eng, and A. J. Hodgson, "Linear spring-damper model of the hypertonic elbow: reliability and validity," *Journal of neuroscience methods*, vol. 128, no. 1-2, pp. 121–128, 2003.

[24] H. K. Khalil and J. Grizzle, *Nonlinear Systems*, vol. 3. Prentice hall, 2002.

Authorized licensed use limited to: New York University. Downloaded on September 08,2024 at 15:00:10 UTC from IEEE Xplore. Restrictions apply.